5-17-2021

# Cyclobutanone Inhibitor of Cobalt-Functionalized Metallo-γ-Lactonase AiiA with Cyclobutanone Ring Opening in the Active Site

Cory T. Reidl
*Loyola University Chicago*

Romila Mascarenhas
*Loyola University Chicago*

Thahani S. Habeeb Mohammad
*Loyola University Chicago*

Marlon R. Lutz Jr
*Loyola University Chicago*

Pei W. Thomas
*University of Texas at Austin*



## Recommended Citation

Reidl, Cory T.; Mascarenhas, Romila; Habeeb Mohammad, Thahani S.; Lutz, Marlon R. Jr; Thomas, Pei W.; Fast, Walter; Liu, Dali; and Becker, Daniel P. Ph.D.. Cyclobutanone Inhibitor of Cobalt-Functionalized Metallo-γ-Lactonase AiiA with Cyclobutanone Ring Opening in the Active Site. ACS Omega, , : , 2021. Retrieved from Loyola eCommons, Chemistry: Faculty Publications and Other Works, http://dx.doi.org/10.1021/acsomega.0c06348

ACS OMEGA

http://pubs.acs.org/journal/acsodf

Article

# Cyclobutanone Inhibitor of Cobalt-Functionalized Metallo-γ-Lactonase AiiA with Cyclobutanone Ring Opening in the Active Site

Cory T. Reidl,[#] Romila Mascarenhas,[#] Thahani S. Habeeb Mohammad, Marlon R. Lutz, Jr., Pei W. Thomas, Walter Fast, Dali Liu,* and Daniel P. Becker*

Cite This: https://doi.org/10.1021/acsomega.0c06348

Read Online

ACCESS | Metrics & More | Article Recommendations | Supporting Information

**ABSTRACT:** An α-amido cyclobutanone possessing a C10 hydrocarbon tail was designed as a potential transition-state mimetic for the quorum-quenching metallo-γ-lactonase autoinducer inactivator A (AiiA) with the support of in-house modeling techniques and found to be a competitive inhibitor of dicobalt(II) AiiA with an inhibition constant of $K_i$ = 0.007 ± 0.002 mM. The catalytic mechanism of AiiA was further explored using our product-based transition-state modeling (PBTSM) computational approach, providing substrate-intermediate models arising during enzyme turnover and further insight into substrate−enzyme interactions governing native substrate catalysis. These interactions were targeted in the docking of cyclobutanone hydrates into the active site of AiiA. The X-ray crystal structure of dicobalt(II) AiiA cocrystallized with this cyclobutanone inhibitor unexpectedly revealed an *N*-(2-oxocyclobutyl)decanamide ring-opened acyclic product bound to the enzyme active site (PDB 7L5F). The C10 alkyl chain and its interaction with the hydrophobic phenylalanine clamp region of AiiA adjacent to the active site enabled atomic placement of the ligand atoms, including the C10 alkyl chain. A mechanistic hypothesis for the ring opening is proposed involving a radical-mediated process.

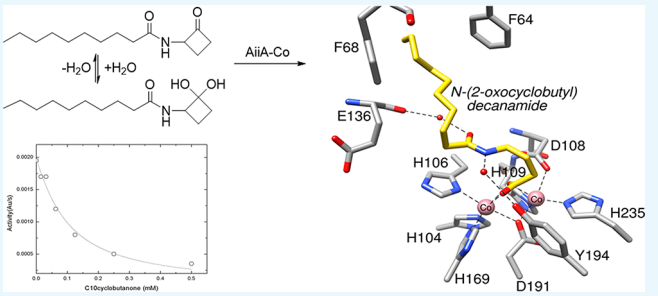




## INTRODUCTION

Bacterial infections are a growing global medical problem, and there is significant interest in the clinical, agricultural, and industrial sectors to understand and manage virulence and to identify and exploit new cellular mechanisms that control pathogenic virulence.[1] Quorum-sensing mechanisms regulate pathways controlling virulence in many Gram-negative bacteria through the production and sensing of autoinducer signaling molecules, such as *N*-acyl-L-homoserine lactone (AHL). The AHL-mediated quorum-sensing pathways have been experimentally linked to the coordinated regulation of virulence factor production, motility, and biofilm formation in pharmacologically relevant bacterial communities.[2] Enzymes that are capable of hydrolyzing the lactone moiety of AHLs are of vital significance due to their ability to disrupt the coordination of communal virulence. These signal-degrading enzymes, known as quorum-quenching (QQ) lactonases, are broadly distributed among Gram-positive bacterial species, although some have been identified in Gram-negative organisms as well.[3−5] Studying their mechanisms of action can provide insight into the role of quorum sensing in virulence as well as designing new antibiotics, perhaps through pharmaceutically enhancing quorum quenching.[6] Autoinducer inactivator A (AiiA), a metalloenzyme first discovered in *Bacillus sp.* strain 240B1,[7] is the best characterized AHL lactonase to date. AiiA[8] is one of several related enzymes in the metallo-β-lactamase superfamily[9,10] that utilize a dinuclear zinc(II) ion metal cluster to catalyze the enzymatic ring hydrolysis of a variety of AHL signaling molecules.[11−15] The general substrate hydrolysis mechanism proposed by Momb et al.[16] is illustrated in Figure 1.

It is critical to enhance our understanding of the mechanisms and functions of quorum-quenching enzymes through structural biology and small molecule modulation of activity. Small molecules that are capable of binding to the active site of AiiA and related enzymes may have the ability to modulate the quorum-quenching mechanism between bacterial communities and provide a valuable chemical tool for studying these systems. *N*-Hexanoyl-L-homoserine lactone (C6-HSL, **1**) and C10-HSL (**3**) are among the most studied homoserine lactone substrates of AiiA and are hydrolyzed to the corresponding homoserine C6-amide **2** and homoserine C10-amide **4**, respectively (Scheme 1).[17,18] Previously, an X-ray crystal structure of the cleaved product **2** of lactone substrate C6-HSL hydrolysis bound to the catalytic metal center (PDB

Received: December 30, 2020
Accepted: April 6, 2021

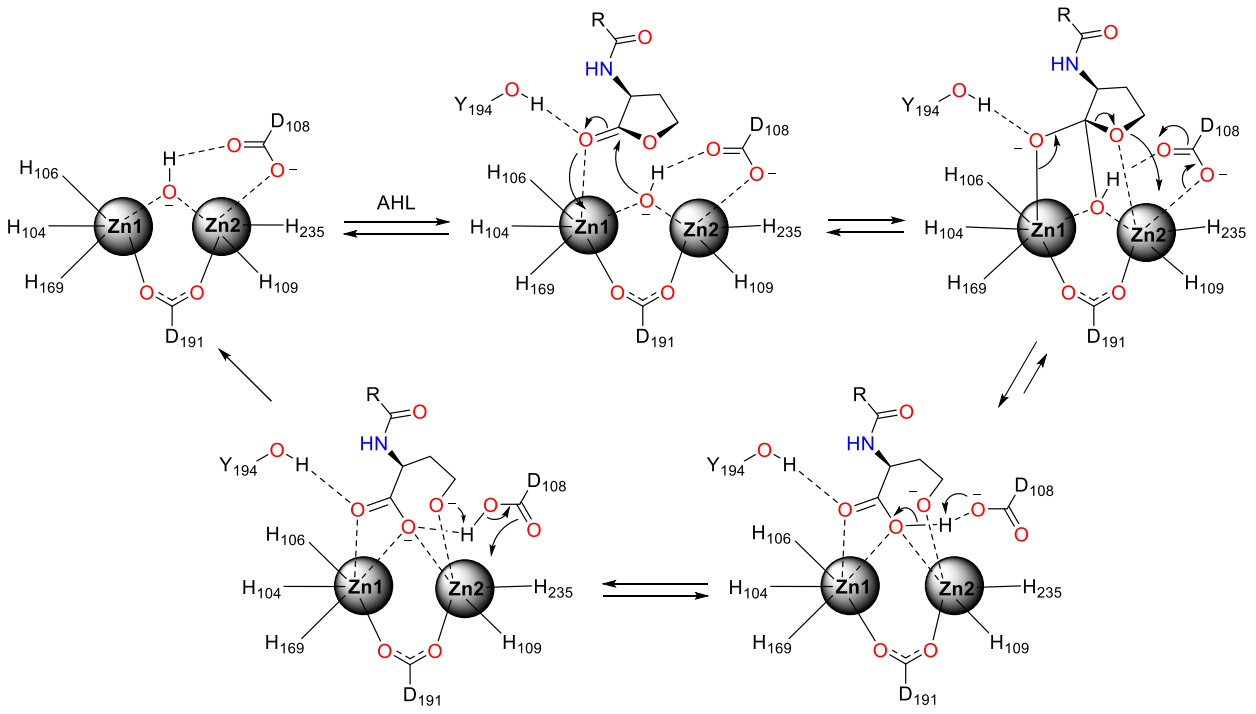


**Figure 1.** Proposed catalytic mechanism of the dizinc AHL lactonase from *Bacillus thuringiensis*.

**Scheme 1. (A) AiiA-Catalyzed Hydrolysis of C6-HSL (1, $K_m$ = 2.1 ± 0.3 mM, di-Zn Cofactor; $K_m$ = 0.36 mM, di-Co Cofactor) and C10-HSL (3, $K_m$ = 0.14 ± 0.5 mM, di-Zn Cofactor; $K_m$ = 0.15 ± 0.02 mM, di-Co Cofactor) to the Corresponding Lactone-Opened Hydroxy Acids 2 and 4, Respectively;[18] (B) C10-Cyclobutanone(±)-5 and the Corresponding Transition-State Mimetic Hydrate(±)-5·$H_2O$**

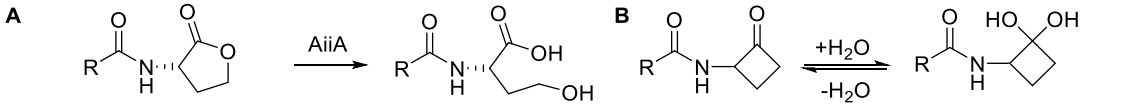


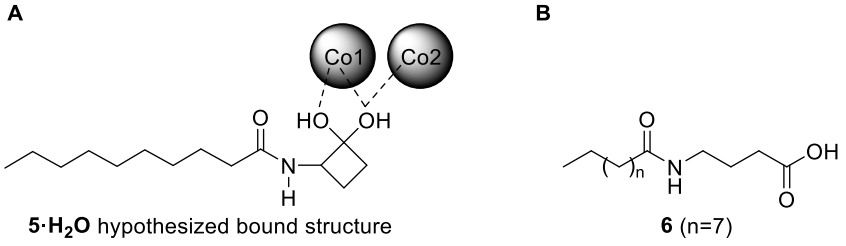


**Figure 2.** (A) Proposed binding of cyclobutanone (±)-5·$H_2O$ to the active site of AiiA-Co and (B) product **6** visualized after X-ray exposure.

3DHB) was reported,[17] as well as a complex structure of the product of C10-HSL lactone hydrolysis bound to the active site, with the C10 tail bound by a phenylalanine clamp (PDB 3DHC).[18] We designed *N*-(2-oxocyclobutyl) decanamide (**5**) as a potential transition-state analogue to study the structure of the proposed tetrahedral intermediate in the mechanism of AiiA HSL hydrolysis and to ultimately study the effect of inhibitors of AiiA as molecular probes for better understanding the role of quorum quenching. The cyclobutanone ring provides a functional group with a degree of conformational rigidity, and the inherent strain of the 4-membered ring makes the ketone carbonyl more electrophilic than the less strained cyclopentyl or cyclohexyl ketone analogues. The hydration equilibrium of cyclobutanones is shifted more toward the hydrate due to this strain, making cyclobutanones a potential transition-state mimetic of hydrolase enzyme intermediates. Strynadka and Dmitrienko reported cyclobutanones as *β*-lactam mimetic micromolar potency inhibitors of metallo-*β*-lactamase IMP-1[19] and also disclosed an X-ray crystal structure of a class B metallo-*β*-lactamase SPM-1 with hydrated cyclobutanone coordinated to the dizinc metal center.[20] We have previously reported inhibition of a serine hydrolase enzyme from *Francisella tularensis* bound as a hemiacetal[21] enabled by the electrophilicity of the cyclobutanone carbonyl, and we recently reported the synthesis and functionalization of a 2-aminocyclobutanone synthon for facile analogue preparation of potential serine protease and metallohydrolase inhibitors.[22] Therefore, we prepared decanoylaminocyclobuta-


https://doi.org/10.1021/acsomega.0c06348
ACS Omega XXXX, XXX, XXX−XXX

none (±)-**5** as a potential transition-state mimetic of homoserine lactone **3**, based on the hypothesized binding of the hydrate of cyclobutanone (±)-**5** [(±)-**5**·$H_2O$] to the dinuclear metal ion active site of AiiA. Earlier studies demonstrated the enzyme activity of dizinc(II), dicobalt(II), dimanganese(II), and dicadmium(II) metalloforms of AiiA and used these isoforms to provide kinetic evidence of a leaving group, metal interaction, assuming that the metalloforms shared a similar catalytic mechanism.[23] Here, we use dicobalt(II) AiiA due to its superior steady-state kinetic parameters to facilitate kinetic studies. However, the X-ray crystal structure of dicobalt(II) AiiA soaked with (±)-**5** did not reveal the expected hydrate but instead indicated a ring-opened cyclobutanone product **6** bound to the metal center (Figure 2).

## EXPERIMENTAL SECTION

All solvents were distilled prior to use, and all reagents were used without further purification unless otherwise noted. All synthetic reactions were conducted under a nitrogen or argon atmosphere. Silica gel 60 Å, 40−75 μm (200−400 mesh), was used for column chromatography. Aluminum-backed silica gel 200 μm plates were used for thin-layer chromatography (TLC). $^1$H NMR spectra were obtained using either a 300 MHz spectrometer or a 500 MHz spectrometer with tetramethylsilane (TMS) as the internal standard, and $^{13}$C NMR spectra were obtained using a 500 MHz spectrometer. High-resolution mass spectrometry (HRMS) spectra were measured on a time-of-flight (TOF) instrument by electrospray ionization (ESI). Decanamide, decanoyl chloride, γ-aminobutyric acid, and bis-(trimethylsilyloxy)cyclobutene were purchased from Sigma-Aldrich (St. Louis, MO). All other reagents for biochemical assays were purchased at the highest quality available.

**Organic Synthesis.** Decanoylamidocyclobutanone (±)-**5** was prepared by reacting decanamide with bis-1,2-(trimethylsilyloxy)cyclobutene under acid catalysis by the general procedure we have previously described (Scheme 2).[24] The decanoylamide of GABA was prepared by reacting decanoyl chloride with 4-aminobutyric acid in the presence of triethylamine.

**Scheme 2. Synthesis of (A) α-Amido Cyclobutanone(±)-5 from Decanamide and 1,2-Bis((trimethylsilyl)oxy)cyclobut-1-ene under Anhydrous Acidic Conditions and (B) the Synthesis of 4-Decanamideobutanoic acid 6**

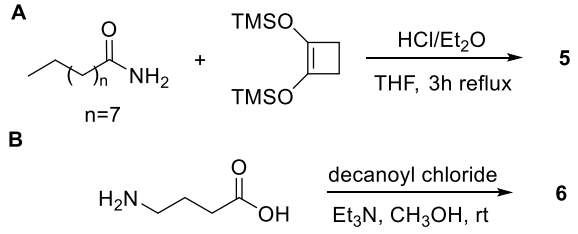


*N-(2-Oxocyclobutyl)decanamide ((±)-5).* According to the general procedure previously described,[24] to a 10 mL round-bottom flask fitted with a condenser were added decanamide (200 mg, 1.17 mmol), 1,2-bis(trimethylsilyloxy)cyclobutene (326 μL, 1.28 mmol), dry tetrahydrofuran (THF) (2.7 mL), and a 1 M solution of HCl in diethyl ether (2.7 mL) at room temperature. The reaction mixture was agitated with magnetic stirring under an inert argon atmosphere and heated to reflux at 55 °C for 3 h after which high-performance liquid chromatography (HPLC) and TLC analysis indicated consumption of the decanamide starting material ($R_f$ = 0.07 in 1:1 of $Et_2O$/petroleum ether). The reaction mixture was concentrated to dryness at atmospheric pressure using a heating bath at 80 °C. The resulting crude syrup was dissolved in diethyl ether and purified by passing through a 4 g silica gel flash cartridge eluted with diethyl ether/petroleum ether (1:1) to afford the title cyclobutanone (±)-**5** (153 mg, 55%) as a white solid: mp 58−59 °C. $^1$H NMR (500 MHz, DMSO-$d_6$) δ 8.28 (d, $J$ = 7.9 Hz, 1H), 4.77 (dtt, $J$ = 10.3, 8.0, 2.4 Hz, 1H), 2.87 (dddd, $J$ = 17.2, 10.6, 8.8, 2.0 Hz, 1H), 2.74 (dddd, $J$ = 17.2, 10.0, 4.5, 2.7 Hz, 1H), 2.18 (qd, $J$ = 10.3, 4.5 Hz, 1H), 2.06 (td, $J$ = 7.2, 1.2 Hz, 2H), 1.97 (tt, $J$ = 10.2, 8.5 Hz, 1H), 1.46 (p, $J$ = 7.3 Hz, 2H), 1.28−1.24 (m, 12H), 0.85 (d, $J$ = 6.2 Hz, 3H).$^{13}$C NMR (500 MHz, DMSO-$d_6$) δ 207.6, 172.3, 64.0, 41.6, 35.2, 31.7, 29.4, 29.2, 29.1, 29.0, 25.6, 22.6, 18.8, 14.4. HRMS $MH^+$ calcd for $C_{14}H_{25}NO_2$: 240.1963, found 240.1952. HPLC purity = 98% monitoring at 220 nm.

*4-Decanamideobutanoic Acid (6).* In an adaptation of the method described by Riva,[25] 4-aminobutyric acid and triethylamine were added to dry methanol in a 20 mL vial. The reaction mixture was cooled to 0 °C over 5 min before decanoyl chloride was added to the vial in 5 portions of 38 μL over 5 min while under a continuous inert gas stream. The reaction vial was sealed and stirred for an additional 1 h at 0 °C before being allowed to warm to room temperature overnight upon which HPLC indicated the consumption of starting material. The reaction mixture was concentrated to dryness before being taken up in 20 mL aqueous HCl (0.5 M). The product was extracted with three 10 mL portions of chloroform, which were combined and dried over sodium sulfate followed by filtration and concentration to dryness under reduced pressure. The resulting white product was dried overnight under high vacuum to afford the title amide **6** (225 mg, 88%) as a white crystalline solid. HPLC of the crude product shows 98% pure without purification: mp 86−87 °C. $^1$H NMR (500 MHz, DMSO-$d_6$) δ 12.00 (s, 1H), 7.77 (t, $J$ = 5.7 Hz, 1H), 3.03 (td, $J$ = 6.9, 5.5 Hz, 2H), 2.20 (t, $J$ = 7.5 Hz, 2H), 2.03 (t, $J$ = 7.4 Hz, 2H), 1.60 (quin, $J$ = 7.2 Hz, 2H), 1.47 (quin, $J$ = 7.1 Hz, 2H), 1.31−1.21 (m, 12H), 0.86 (t, $J$ = 6.9 Hz, 3H). $^{13}$C NMR (500 MHz, DMSO-$d_6$) δ 174.7, 172.5, 38.2, 35.9, 31.7, 31.5, 29.4, 29.2, 29.1, 29.1, 25.8, 25.1, 22.6, 14.4. HRMS $MH^+$ calcd for $C_{14}H_{27}NO_3$ 258.2069, found 258.2058.

**Computational Chemistry.** Calculations at the density functional level of theory were performed using Spartan '016 by Wavefunction, employing the M06 2X functional and the 6-31 basis set as generally described.[26]

**Inhibition Assay.** The rate of substrate hydrolysis in the presence of the cyclobutanone inhibitor was monitored using a previously described continuous spectrophotometric assay[27] in which the pH indicator phenol red acts as part of the assay buffer [1 mM 4-(2-hydroxyethyl)-1-piperazineethanesulfonic acid (HEPES) (pH 7.5)] and results in a change in the colorimetric signal upon protonation by the net release of a proton upon lactone hydrolysis. Stock solutions of the substrate (C7-HSL) and (±)-**5** were prepared in methanol. Continuous spectrometric kinetic assays were used to determine the initial hydrolysis rate by mixing substrate (0.5−2.5 mM) and inhibitor (0.015−0.5 mM) with an assay buffer in a 1 mL polystyrene cuvette. The addition of a 50 nM


https://doi.org/10.1021/acsomega.0c06348
ACS Omega XXXX, XXX, XXX−XXX

purified enzyme initiated each reaction, which was monitored continuously at 557 nm. The absorbance change monitored over 30 seconds was used to calculate the initial velocity. The Michaelis–Menten equation $V = V_{max}\cdot S/(S + K_m)$, a modified Hill equation $V = V_{max}\cdot I^n/(IC_{50}{}^n+I^n)$, and the Cheng–Prusoff equation $K_i = IC_{50}/(1 + S/K_m)$ were used to obtain $K_m$, $IC_{50}$, and $K_i$, respectively, to evaluate the potency of inhibition.

**Crystallization.** Earlier work has shown that dicobalt-substituted AHL lactonase, AiiA-Co, from *B. thuringiensis* exhibits hyperactivity; therefore, AiiA-Co was prepared as previously described.[23] The purified AiiA-Co protein was exchanged into 50 mM HEPES buffer pH 7.0 and concentrated to 20 mg/mL using an Amicon-Ultra (30000 MWCO), centrifugal filter device (Millipore, MA). Protein crystallization was carried out in hanging drops using modified published conditions for AiiA-Zn.[28] Crystals were obtained from the solution containing 160 mM $MgCl_2\cdot 6H_2O$, 80 mM bis–Tris pH 8.5, 24% w/v PEG 4000, using a protein:well solution ratio of 1:1. Crystals appeared within a week when incubated at 20 °C, along with slight precipitation. AiiA-Co crystals with the best morphology were soaked overnight in a well solution containing 25 mM of **(±)-5** and 25% glycerol and cryocooled in liquid nitrogen.

**Data Collection and Processing.** Monochromatic data sets were collected at the 19-BM beamline at SBC, Advanced Photon Source (APS) at Argonne National Laboratory (ANL). Diffraction data were collected at a wavelength of 0.98 Å at 100 K using an ADSC Quantum 210r CCD detector. Data were indexed and integrated using HKL3000.[29] The best data set was processed at a resolution of 1.54 Å. Data collection statistics are summarized in Table S2.

**Structure Determination, Model Building, and Refinement.** AiiA-Co was soaked with cyclobutanone **(±)-5**, and the crystal structure of the AiiA-Co: *N*-(2-oxocyclobutyl) decanamide complex was solved by molecular replacement using PHASER in the Phenix software suit.[30] The initial search model was based on a previously published structure of AiiA-Zn (PDB ID: 2A7M). Models were rebuilt using COOT[31] and refined using the program Phenix and analyzed using the programs COOT and UCSF Chimera.[32] Ligands were built and regularized using the software JLigand[33] and fit into the difference density in COOT. Structural figures were made using UCSF Chimera.[32] Refinement statistics are summarized in Table S2.

**Molecular Docking.** Ligand models of the (*R*)- and (*S*)-decanoylamidocyclobutanone enantiomers of **(±)-5** as well as the corresponding (*R*)- and (*S*)-decanoylamidocyclobutanone hydrate enantiomers of **(±)-5·H$_2$O** were generated using the molecular operating environment[34] (MOE) computational suite's Builder utility followed by minimization in the gas phase using the force field MMFF94X. The minimized ligands were then subjected to the conformational search protocol to generate structural-conformation databases populated with as many as 10,000 individual conformations. Conformational databases were generated for all ligands of interest for use in the following docking experiments.

The AiiA X-ray crystal structure (PDB ID: 3DHB) containing the hydrolyzed product **2** was first uploaded into MOE. The catalytic Zn(II) ions in the original structure were converted to Co(II), and the product structure was deleted from the system. The prepared apo-AiiA-Co system was then solvated in a simple water box at a pH of 7.4 with periodic boundaries enabled. The hydrogen-bonding network of the solvated system was further optimized by automatically sampling different tautomer/protomer states using the Protonate3D utility in MOE, which calculates optimal protonation states, including titration, rotamer, and "flips" using a large-scale combinatorial search. The apo-AiiA-Co system was then minimized and subjected to a 2200 ps simulated annealing experiment to prepare the receptor for molecular docking.

Following the preparation of the docking receptor model, molecular docking was performed using the previously generated ligand conformation databases. Analogue docking was carried out in the prepared AiiA-Co enzyme model with the solvent atoms inactivated and the docking site specified at the catalytic Co(II) atoms and active-site binding cleft.[17] Ligand placement employing the proxy triangle method with London dG scoring generated 50 docking poses that were further refined to the top 30 docking results using the induced fit method with GBVI/WSA dG scoring. The best docking pose for each ligand of interest was selected for further model optimizations.

The docked models were resolvated in a water box at a pH of 7.4 and treated with NaCl counterions to balance the charge. Periodic boundary conditions were enabled, and the hydrogen-bonding network of each model was optimized using Protonate3D. The system atoms were then optimized with a short, localized molecular minimization process with atoms further than 10 Å from the substrate fixed. System refinement continued until an RMS gradient of 0.1 kcal/(mol Å) was attained. Molecular dynamics (MD) parameters were set to globally minimize the protein, substrate, and solvent atoms in the system using an NPA algorithm with an Amber12:EHT force field, with heating and cooling protocols. The simulation results were then minimized once again before the final binding poses were obtained for comparison.

**In Silico Modeling.** Product-based transition-state modeling (PBTSM)[35,36] was performed using the chemical computing group's molecular operating environment[34] (MOE). Two *Btk* AiiA crystal structures (PDB entries 3DHB and 4J5H), bound with **2** and **4**, respectively, were used as the starting points for PBTSM. The crystal structures were prepared using MOE's structure-prep utility. In the case of 4J5H, a mutant F107W AiiA structure, W107, was initially mutated back to the native F107 residue using the Protein Builder utility in MOE. Each model was solvated in a simple box of water at pH 7.4 that contained NaCl counterions for charge balance. Periodic boundary conditions were enabled, and the hydrogen-bonding network of the model was optimized by sampling different tautomer/protomer states using Protonate3D.[37] A localized energy minimization was run on the solvated systems using the MOE function QuickPrep, followed by a short global minimization to equilibrate the system, and subsequent 0.5 ns molecular dynamics (MD) equilibration using an NPA algorithm with an Amber14:EHT force field. The molecular dynamic experiments performed utilized an initial heating stage from 0 to 311 K over 100 ps followed by an equilibration stage for 100 ps at 311 K and a 200 ps production stage, concluding with a cooling stage from 311 to 0 K over 100 ps. Using the accepted mechanism outlined in Figure 1 as a guide, the atom coordinates of the bound products, **2** and **4**, respectively, were used as initial starting points to model the proton transfer steps from the hydroxyl moiety onto the carboxylate of the bound product via the general acid–base catalyst D108, followed by the


https://doi.org/10.1021/acsomega.0c06348
ACS Omega XXXX, XXX, XXX–XXX

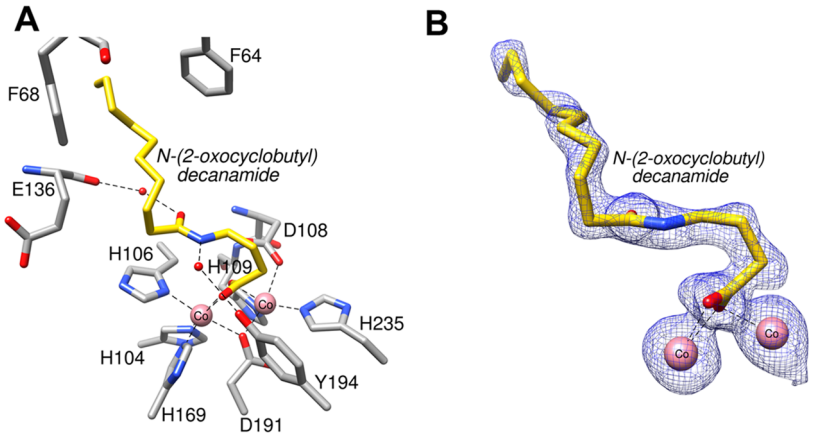


**Figure 3.** Active site of AiiA-Co bound to **6**. (A) Side-chain atoms representing the protein are shown in gray, and the metal atoms (cobalt) are shown in pink. Heteroatoms oxygen and nitrogen are represented in red and blue, respectively, and **6** is shown in yellow. Panel (B) represents an Fo−Fc omit map shown as a blue mesh at 3$\sigma$.

tetrahedral transition state intermediate, the subsequent substrate-catalytic hydroxyl-bound structures, and the initial substrate binding model. At each stage of the protocol, the hydrogen-bonding network and formal charges were optimized to maintain a balanced overall net charge of the system. Localized minimization followed by global minimization was conducted before and immediately after applying a 1.0 ns MD equilibration to each intermediate model generated, as previously described.

## RESULTS AND DISCUSSION

**Inhibition of AiiA-Co by *N*-(2-Oxocyclobutyl)-decanamide ((±)-5).** We hypothesized that cyclobutanone (±)-**5**, as its corresponding hydrate (±)-**5**·$H_2O$, is capable of mimicking the tetrahedral transition state of the lactone hydrolysis of the AiiA $\gamma$-lactone substrate. We conducted kinetic inhibition assays to test the effects of (±)-**5** on the activity of AiiA-Co using a previously described continuous assay to assess the inhibitory potency of (±)-**5** on the activity of AiiA-Co by plotting activity versus concentration of (±)-**5**. Inhibition assays were carried out at substrate *N*-heptanoyl-L-homoserine lactone (**C7-HSL**) concentrations of 0.5, 1.0, and, 2.5 mM, and the $IC_{50}$ values of inhibitor (±)-**5** were found to be 0.06 ± 0.02, 0.10 ± 0.03, and 0.38 ± 0.04 mM, respectively (Figure S7). The plots of activity versus concentrations of the inhibitor (±)-**5** (Figure S7) show that the $IC_{50}$ value increases with an increase in the concentration of a substrate. These data are consistent with proposing that decanamidecyclobutanone (±)-**5** acts as a competitive inhibitor of AiiA.

A $K_m$ value of 0.07 ± 0.003 mM for substrate C7-HSL was obtained using a Michaelis−Menten fit in the absence of the compound (±)-**5**. According to the Cheng−Prusoff equation and using the obtained $K_m$ and $IC_{50}$ values, the inhibition constant was calculated as $K_i$ = 0.007 ± 0.002 mM, which is ∼10 times smaller than the $K_m$ displaying potent inhibition. Compound (±)-**5** also shows a relatively high affinity for dicobalt(II) AiiA when compared with other published AiiA ligands. Product inhibition for the dizinc(II) and dicadmium-(II) metalloforms of AiiA was previously determined for *N*-hexanoyl-L-homoserine (2Zn: no inhibition ≤25 mM; 2Cd: $K_i$ = 2 mM) and *N*-hexanoyl-L-homocysteine (2Zn: $K_i$ = 550 $\mu$M; 2Cd: $K_i$ = 3 $\mu$M).[17,23] Inhibitor (±)-**5** has a much greater affinity for dicobalt AiiA than each of these other complexes, except for *N*-hexanoyl-L-homocysteine and dicadmium(II) AiiA, which likely stems from a strong thiolate−Cd(II) coordination. Additionally, a substrate with the same N-acyl chain length as (±)-**5**, *N*-decanoyl-L-homoserine lactone has a higher $K_m$ value (150 $\mu$M) when compared to the $K_i$ of (±)-**5**.[16] The synthesized compound **6** was tested for inhibition; no inhibition was detected up to 0.5 mM of compound **6** (Figure S8). Since the calculated inhibition constant for compound (±)-**5** based on the Cheng−Prusoff equation is ∼71 times smaller, we hypothesize that the inhibition of compound (±)-**5** is caused by the hydrated tetrahedral form. Consistent with this conclusion is the fact that the bound conformation of **6** in the crystal resembles the butanone ring rather than a more extended conformation (Figure 3).

**Complex Structure of 4-Decanamidobutanoate (6)-Bound AiiA-Co.** We performed X-ray crystallography experiments to gain structural insight into the mechanism of inhibition of AiiA by cyclobutanone (±)-**5**, which unexpectedly provided the bound, ring-opened structure **6** in the active site of AiiA-Co (PDB 7L5F). The structure of **6**-AiiA-Co, derived from soaking AiiA-Co with cyclobutanone (±)-**5**, was solved by molecular replacement using a monomer of the known AiiA-Zn structure as a search model (PDB: 2A7M) after deleting all water and ligand molecules in the space group $P2_12_12_1$. Multiple cycles of model building and refinement were conducted, and the final model was refined to a resolution of 1.51 Å with $R_{work}/R_{free}$ values of 14.95/17.00. The final refinement statistics are detailed in Table S2.

There are no changes in the overall protein structure of **6**-AiiA-Co when compared to that of apo-AiiA-Zn (rmsd = 0.19 Å) (PDB ID = 2A7M). The difference density at the active site after model building and refinement of the protein and solvent molecules was interpreted as 4-decanamideobutanoic acid (**6**) bound in the active site (Figure 3). Figure 3B shows a simulated annealing omit map (Fo−Fc) at 3.0 $\sigma$ superimposed with a model of **6**. The C10 acyl tail of **6** occupies a hydrophobic cavity that is flanked by residues F64 and F68 creating a phenylalanine clamp to stabilize substrate binding. This mode of product binding has been observed in the crystal structure of AiiA bound to *N*-decanoyl-L-homoserine (**4**) and is favored for substrates containing C7 or longer alkyl chains,[18] with C6 or shorter alkyl chain substrates occupying an adjacent


https://doi.org/10.1021/acsomega.0c06348
ACS Omega XXXX, XXX, XXX−XXX

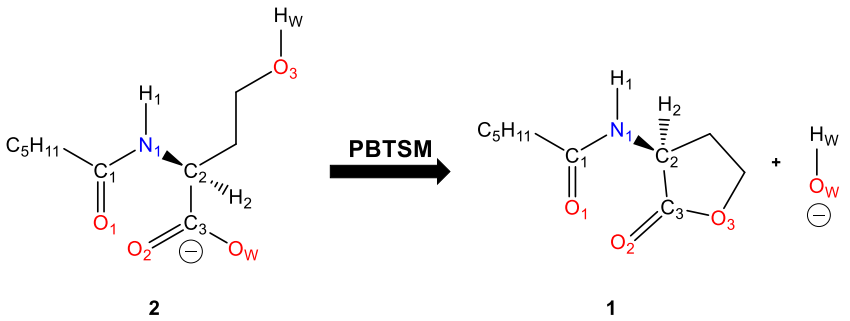


**Figure 4.** Overall product to substrate structure conversion via PBTSM with atoms labeled for reference.

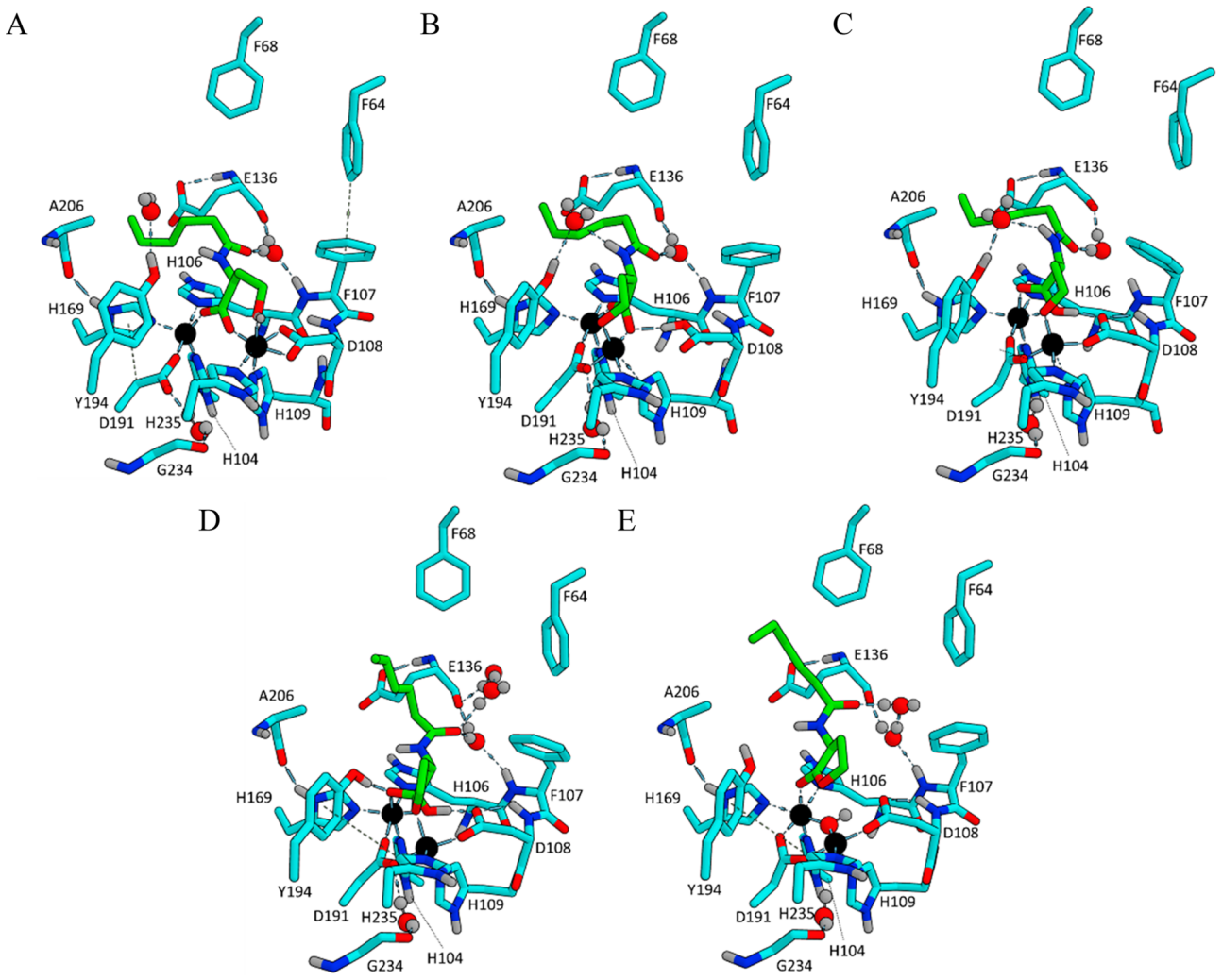


**Figure 5.** PBTSM-generated models showing the metal-binding pocket of (A) AiiA-Zn atoms interacting with the ring-opened product homoserine **2**, (B) D108 carboxylic acid of AiiA-Zn with homoserine **2**-$O_3^-$, (C) AiiA-Zn with HOOC-**2**-$O_3^-$, (D) AiiA-Zn bound with the transition-state complex of **2**, and (E) AiiA-Zn bound with **1** and the activated catalytic hydroxyl group. The Zn(II) ions are shown as black spheres and waters as red spheres; amino groups are colored dark blue and red for nitrogen and oxygen, respectively. See Figure S10A–E for corresponding stereoviews.

hydrophobic pocket as seen in the structure of AiiA bound to **2**.[17]

The residue Y194 has been postulated to play an important role in AiiA catalysis, stabilization of a proposed tetrahedral intermediate, and is observed making hydrogen bonds to **6** via a bridging water (Figure 3a).[16] The structure of the active site of AiiA bound to **6** shows an apparent cleavage of a C–C bond that occurred during crystal soaking or data collection of (±)-**5** in complex with AiiA-Co. It is uncertain whether the ring-opening reaction occurred because of catalysis by the enzyme while soaking AiiA crystals with (±)-**5** or due to X-ray radiation during data collection. We favor the latter hypothesis.

In the crystal structure of AiiA-Zn bound to product **2** (PDB ID: 3DHB), a water molecule bridges the two Zn atoms at the active site. This structure has been proposed to represent the active site of AiiA during product release and regeneration with the bridging water.[17] However, in the crystal structure of **6**-AiiA-Co, we do not see a bridging water in the active site at


https://doi.org/10.1021/acsomega.0c06348
ACS Omega XXXX, XXX, XXX–XXX

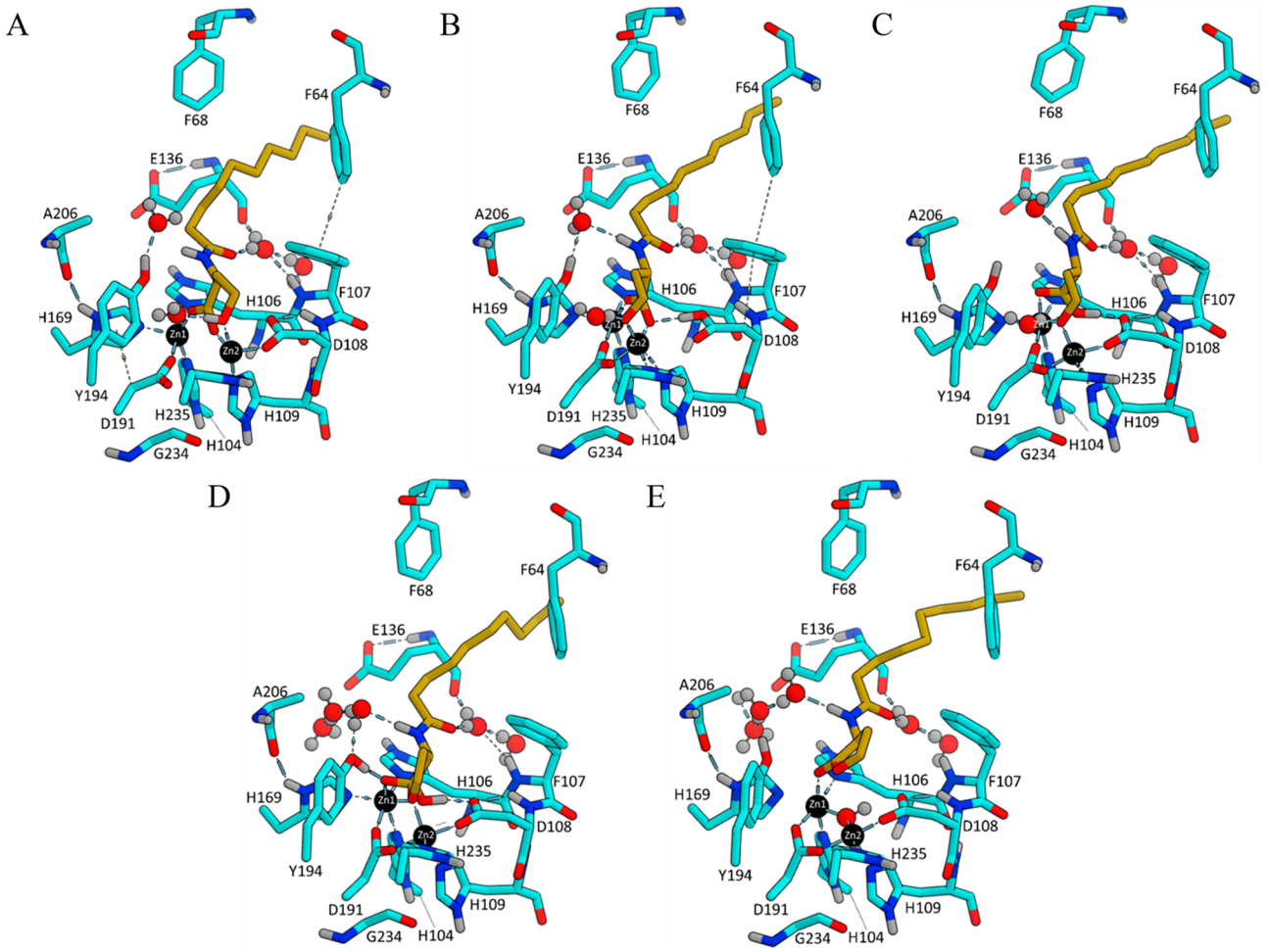


**Figure 6.** PBTSM-generated models showing the metal-binding pocket of (A) AiiA-Zn atoms with the ring-opened product homoserine **4**, (B) D108 carboxylic acid form of AiiA-Zn with homoserine **4**-$O_3^-$, (C) AiiA-Zn with HOOC-**4**-$O_3^-$, (D) AiiA-Zn bound with the transition-state complex of **4**, and (E) AiiA-Zn bound with **3** and the activated catalytic hydroxyl group. See Figure S11A−E for corresponding stereoviews.

AiiA. This position is likely occupied by one of the carboxylate oxygen atoms of **6** (Figure 3). Given our interest in enzyme inhibitors and enzymatic mechanisms, and to gain insight into the binding of (±)-**5**·$H_2O$, we sought to further examine the mechanism of homoserine lactone ring opening by AiiA through application of our recently developed product-based transition-state modeling protocol.

**Enzyme Mechanism Modeling.** We applied our recently reported product-based transition-state modeling (PBTSM)[35,36] method to the product-bound AiiA crystal structures available (C6-HSL/3DHB and C10-HSL/4J5H) to gain insight into the reported enzyme kinetic data, elucidate potential roles of active-site residues in substrate binding and catalysis, and use these insights to design molecules capable of inhibiting the enzyme. Figure 4 shows the overall product to substrate structure conversion analyzed via PBTSM with key atoms labeled for reference. The PBTSM method proceeds in a reverse chronological reaction order beginning with reaction products and progresses back through known reaction intermediates to the original substrate. Thus, PBTSM is an approach that provides informative models of the lowest-energy structure at each major stage of a given catalytic cycle through a combination of molecular mechanics and molecular dynamics utilities. The PBTSM protocol was developed using the molecular operating environment (MOE) computational suite,[34] and we applied this method to a product-bound GCN5-related *N*-acetyltransferase (GNAT) PA4794 enzyme[35] and to the dizinc bacterial enzyme diaminopimelate desuccinylase (DapE).[36] In the present study, we apply this methodology to the two previously reported AiiA product-bound crystal structures (PDB IDs: 3DHB and 4J5H) with enzymatically hydrolyzed products **2** and **4**, respectively. The original atomic coordinates from the PDB structures, **2**-AiiA-Zn and **4**-AiiA-Zn, were used to model the catalytic intermediate models (Figure 5A−E for **2** and Figure 6A−E for **4**; Figures S10A−E and S11A−E, respectively, for stereoviews) associated with proton ($H_W$) shuttling events from the product alcohol oxygen ($O_3$) to the product's carboxylate oxygen ($O_W$) via protonation and deprotonation of the general acid−base catalyst D108, which are assumed to take place following decomposition of the tetrahedral transition-state complex.

For the originally reported C6 product **2**-AiiA-Zn structure, system preparation, solvation, and initial minimization to relax the crystal packing were carried out. The carboxylate oxygen atoms ($O_2$) and ($O_W$) of **2** remained bidentate-bridged between the Zn1 and Zn2 atoms, respectively. The amide carbonyl oxygen ($O_1$) also hydrogen-bonds to a structural water referred to as $H_2O_a$, which itself is held in place by backbone hydrogen bonding with the F107 amido hydrogen


https://doi.org/10.1021/acsomega.0c06348
ACS Omega XXXX, XXX, XXX−XXX

and E136 carbonyl oxygen, while the amide bond of product **2** forms a solvent-mediated interaction with the hydroxyl moiety of Y194 via a second structural water ($H_2O_b$). Energy minimization of the system results in the formation of metal-binding interactions to Zn2 by the oxygen atom ($O_3$) of the hydroxyl moiety ($O_3$−$H_w$). Finally, the 5-carbon alkyl chain atoms of **2** occupy the solvent-exposed channel of the Y-shaped active-site cavity.[17] Energy minimization also causes the tail of **2** to gain favorable hydrophobic interactions via the proximity to the backbone residues A206, G207, and F208, in addition to the side-chain moieties of H106, H169, S170, and E136.

The prepared, solvated, and minimized C10 product **4**-AiiA-Zn structure, on the other hand, experiences more structural deviations from the original crystal structure during the initial model preparation. This is due, in large part, to the W107F → F107 retromutation that was applied to the system. Before the modeling of **4**-AiiA-Zn, the product−enzyme interactions are nearly identical to that described for **2**, with the exception that the hydroxyl moiety of **4** (**4**-$O_3$−$H_w$) forms a hydrogen bond to the sulfur atom of C14 near the mutant residue W107 and the placement of the 9-carbon alkyl tail moiety of **4**, which occupy the phenyl clamp region of the AiiA's Y-shaped cavity due to favorable interactions with the side-chain phenyl rings of F68 and F64, in addition to I73, V69, T67, G136, and M138. After retromutation to form the **4**-AiiA-F107-Zn model (**4**-AiiA-Zn), the system was solvated, followed by minimization and annealed with molecular dynamics. Following these manipulations to the system, hydrogen bonding was lost between the side chain of C14 (Cys14) and the atoms of **4**'s hydroxyl moiety (**4**-$O_3$−$H_w$), which instead coordinates with Zn2 where $O_3$−$H_w$ can participate in proton transfer to the side chain of the D108.

Using the prepared product-bound models of **2**-AiiA-Zn and **4**-AiiA-Zn as starting points, the Builder utility of MOE was used to model the transfer of $H_W$ from $O_3$ to the side-chain carboxylate of D108 resulting in the D108-COOH_AiiA-Zn model (Figures 5B and 6B) complexed with deprotonated product intermediates **2**-$O_3^-$ or **4**-$O_3^-$, respectively. In both cases, the strengthened complexation of the $O_3^-$ atom to Zn2 as well as H-bond formation between $O_W$ and D108's carboxylic acid $H_W$ atom resulted following energy minimization and molecular dynamics equilibration of the system using an NPA algorithm with an Amber14:EHT force field. These two new models reflect the moment immediately after the transfer of $H_W$ from D108 to $O_W$, of the bound product, but before the D108 side chain can transfer $H_W$ to $O_3$ through movement in the side-chain carboxylic acid of D108. Although this motion is not captured in this modeling, it can be inferred by examination of the alternative conformation at D108 (PDB 3DHB-B; not depicted), which is in a 1:1 occupancy with the conformation portrayed in Figures 5B and 6B.

The Builder utility was once again used to model a second proton transfer between the side-chain carboxylic acid of D108 and the $O_W$ atom of the bound products, resulting in AiiA-Zn models (Figures 5C and 6C) complexed with intermediates HOOC-**2**-$O_3^-$ and HOOC-**4**-$O_3^-$, respectively, after minimization and molecular dynamics. These models reflect the moment just after the breaking of the bond between the $C_2$−$O_3$ bond and decomposition of the tetrahedral transition-state complex.

With the minimization of the two intermediate-bound enzyme systems complete, the generated atom coordinates were used to model the tetrahedral transition-state complexes of **2** and **4**, respectively. These models reflect the moment immediately after the nucleophilic attack by the hydroxyl group ($O_W$−$H_W$) at the ester carbonyl carbon ($C_2$) of the substrate (Figures 5D and 6D). The scissile carbonyl carbon is a 2.9 Å Zn-bound $O_3$ atom of **2** or **4** in the AiiA-Zn product-bound structure (Figures 5C and 6C), whereupon re-formation of the ester bond using the Builder utility in MOE creates a distorted tetrahedral intermediate complex. A correction to the formal charge of the alkoxide oxygen ($O_2$), associated with ester carbonyl polarization upon attack by the catalytic hydroxide, was concomitantly applied to the complex. Following H-bond network optimization and a local minimization to normalize the bond distances and angles of the tetrahedral intermediate, as well as balance the net charges of the ligand/receptor system, a molecular dynamics equilibration was again applied to the system.

Analysis of the tetrahedral **2**-TS- and **4**-TS-bound intermediate models reveals several aspects of the catalytic mechanism, which provided valuable insight into the early stages of designing the hypothesized transition-state mimetic (±)-**5**. First, a difference in the solvent molecule stabilized between the intermediates amide hydrogen (H1) and the oxygen atoms of the Y194 side chain is observed between **2** and **4**. This likely occurs because the high degree of flexibility in the shorter substrate's (**2**'s) hydrophobic alkyl tail, as it sits loosely in the larger binding cleft of the Y-shaped cavity, pushes solvent molecules away from the substrates NH atoms and Y194 hydroxyl atoms to strengthen more constructive hydrophobic interactions with the nearest hydrophobic residues, the side chains of Y194 and A206. This action discourages H-bonds from forming between these two species. Although we did not observe the formation of structured water between the amide and Y194, our modeling does not preclude its formation in vivo. However, our results do suggest that this behavior likely contributes to the reduced binding affinity and increased $K_m$ values observed experimentally for substrates with shorter tailed lengths. Conversely, the longer tail chain length of **4** allows it to take advantage of hydrophobic interactions with the phenyl clamp region of the Y-shaped binding cleft, thus lowering the entropy of the system and preventing disordering of solvent molecules between the substrate and enzyme.

To complete the catalytic mechanism sequence, the PBTSM methodology was again applied to the tetrahedral TS-bound models to provide the atomic coordinates for the catalytic hydroxyl group and native substrate, **1** and **3**, respectively, bound to AiiA-Zn (Figures 5D and 6D). MOE's Builder utility was used to remove the bond between the tetrahedral carbonyl carbon ($C_2$) and the $O_W$ atom of **2**-TS and **4**-TS complexes, respectively. Manual ionization-state adjustment of the newly formed catalytic water/hydroxide oxygen to a negative form ($O_2^-$−$C_2$···X···$O_W$−$H_W$ to $O_2^-$−$C_2$ + $^-O_W$−$H_W$) and a double bond was created to re-form the substrate carbonyl moiety ($O_2^-$−$C_2$−$O_3$ to $O_2$=$C_2$−$O_3$). A local minimization followed by a global minimization was initiated to correct bond angles and distances, after which a 0.5 ns molecular dynamics equilibration was performed (Figures 5E and 6E). Thus, the catalytic hydroxyl group was modeled into the system. These two models were compared to the previously reported[16] QM-MM model of **1** bound to the catalytic hydroxyl/Zn species of AiiA and were found to be in close agreement with only slight deviations in Zn−Zn distances.


https://doi.org/10.1021/acsomega.0c06348
ACS Omega XXXX, XXX, XXX−XXX

**Scheme 3. Proposed Mechanism of Cyclobutanone Ring Opening**

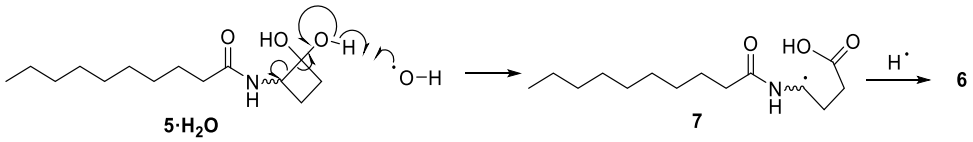


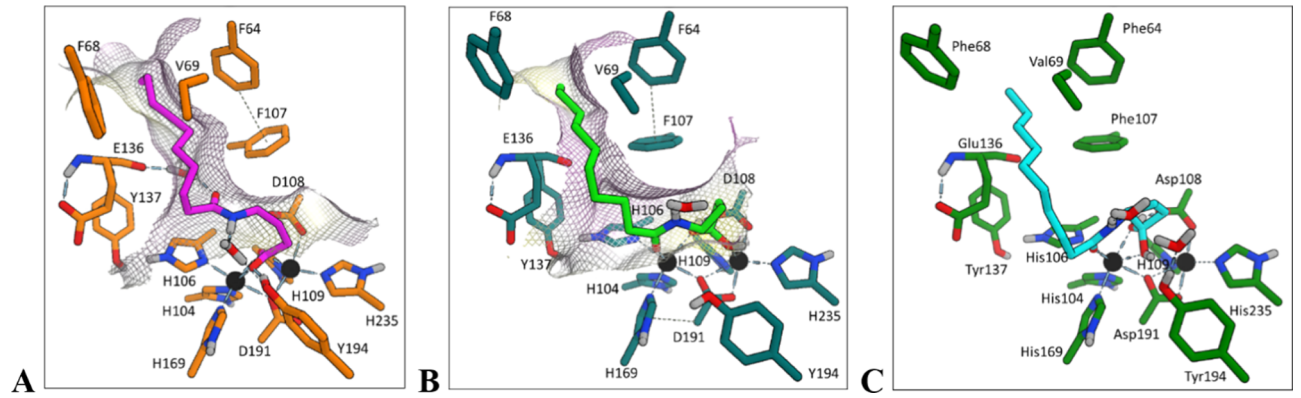


**Figure 7.** (A) Ring-opened product **6** bound to the crystal structure of AiiA-Co. (B) Docking model of (*R*)-5·$H_2O$ bound to equilibrated AiiA-Co. (C) Docking model of (*S*)-5·$H_2O$ bound to the equilibrated AiiA-Co.

**HPLC Analysis to Test the Formation of Ring-Opened Analogue via an Enzyme-Mediated Mechanism.** We hypothesize that the cyclobutanone ring opening occurs via a radical-mediated process initiated by the production of hydroxyl radicals during X-ray irradiation and data collection, as hydroxyl radicals are known to be produced during the process of irradiation.[38] Specifically, H-atom abstraction by a hydroxyl radical (Scheme 3) could induce fragmentation affording a carbon-based radical (**7**) that is strongly stabilized[39] by the substituent amido group. We explored the possibility of the formation of the ring-opened product (**6**) mediated by the enzyme in the absence of X-ray irradiation. We performed a discontinuous HPLC assay to examine this option (see the Supporting Information, SI, for details). However, we found no evidence of ring opening in the presence of AiiA-Co alone.

The ring opening of the cyclobutanone is highly exothermic through the release of strain in the 4-membered ring. The heat of formation of the ring-opened 4-decanamideobutanoic acid **6** was calculated to be 25.0 kcal/mol more stable than the isomeric cyclobutanone hydrate ((±)-5·$H_2O$), as determined by density functional theory (DFT) calculations employing the M06 2X functional and the 6-31 basis set according to a general method described previously.[26]

**Forced Degradation Studies of Decanoylamidocyclobutanone (±)-5.** Follow-up experiments were performed to determine whether the presence of the observed ring-opened product originated from radiation damage during crystallographic data collection. Various reactions were performed with cyclobutanone (±)-**5**, and the formation of the ring-opened decanoylamide carboxylic acid **6** was assayed. Briefly, cyclobutanone (±)-**5** was subjected to reaction screening with radical initiators, including AIBN and $H_2O_2$, as well as in the presence of various metal salts (see the SI for details). Finally, cyclobutanone (±)-**5** was subjected to X-ray exposure (Figure S9 and Table S3) and monitored for the formation of **6** via high-performance liquid chromatography (HPLC). However, the ring-opened product was again not observed (see the SI for details).

While ring-opening reactions of cyclobutanones are well known,[40] the only example of an α-heteroatom-substituted cyclobutanone ring opening to a butyric acid derivative that we are aware of is of 2,2-dibromocyclobutanone opening to give 4,4-dibromobutyric acid when treated with strongly nucleophilic alkanoates including methoxide,[41] whereas the only similar fragmentation of an α-aminocyclobutanone derivative was observed photochemically.[42] We sought to explore conditions that might promote the opening of cyclobutanone (±)-**5** to give **6** including Fenton's reagent[43] that initiates the production of hydroxyl radicals in situ, but the treatment of cyclobutanone (±)-**5** under these conditions gave no detectable trace of **6** by HPLC, which is perhaps not surprising given the highly reactive properties of Fenton's reagent, which could further degrade the compound. Forced degradation of cyclobutanone (±)-**5** with either pyridine N-oxide or with the free-radical TEMPO also did not yield **6** ($MH^+$ = 258) by HPLC/MS but rather afforded a product of a probable Baeyer−Villiger oxidation and hydrolytic ring opening.

**Molecular Docking.** To further understand how our inhibitor binds to AiiA and how the enzyme may facilitate the observed ring-opening mechanism of (±)-**5**, we have developed a series of molecular models of the expected cyclobutanone hydrates in complex with AiiA using classic molecular docking and dynamic techniques. To accomplish this task, we first generated an equilibrated receptor model using the previously solved crystal structure of **6**-AiiA-Co as our base model. We removed the ligand structure of **6** from the model leaving only the apo-AiiA dicobalt receptor. The apo-AiiA dicobalt system was solvated in a water box and equilibrated for 200 ps to relax the crystal packing and used as the docking receptor for subsequent docking experiments.

Ligand conformational databases for (*R*)-5·$H_2O$ and (*S*)-5·$H_2O$ were prepared as previously described and used to generate docking poses of the ligands of interest bound at the metallo centers of AiiA. Docking poses for (*R*)-5·$H_2O$ and (*S*)-5·$H_2O$, respectively, were selected based on the proximity of the alkyl tail to the hydrophobic phenyl clamp region and the


https://doi.org/10.1021/acsomega.0c06348
ACS Omega XXXX, XXX, XXX−XXX

strength of the metal binding at the di-metallo center. Each docking model was further optimized by subsequent solvation, equilibration, and minimization to give the final models for analysis, as seen in Figure 7.

Comparison of the docking results for (*R*)-**5**·$H_2O$ and (*S*)-**5**·$H_2O$ (Figure 7b,c, respectively) with the original **6**-AiiA-Co structure (Figure 7a) shows the characteristic interaction of the alkyl tail with the hydrophobic phenyl clamp region as expected. Additionally, the docking poses of (*R*)-**5**·$H_2O$ and (*S*)-**5**·$H_2O$ were found to form three-point coordination with the metal center. In the case of (*R*)-**5**·$H_2O$, a bidentate interaction is formed between Co1 and the lone pair electrons of the amide carbonyl and the oxygen atoms of one of the hydrate groups, which itself forms a hydrogen bond interaction with the carboxylate of D108, while the opposing hydrate oxygen interacts with Co2. However, in the case of (*S*)-**5**·$H_2O$, we see a three-coordinate binding interaction in the form of chelation between Co1 and the amide carbonyl and both hydrate oxygen atoms. These docking results suggest that either configuration of **5** would be recognized by AiiA.

Analysis of the active-site residues surrounding the docked ligands suggests a possible explanation for why the cyclobutanone ring-opening event has thus far only been observed upon X-ray radiation exposure of cocrystallized **5**-AiiA and not from other experimental conditions tested. In AiiA, the Y-shaped active-site cavity makes the side-chain hydroxyl group of Y194 relatively solvent-exposed and easily accessible to hydroxyl radicals propagating through bulk solvent once generated. Tyrosine residues are generally accepted to be good redox-active species, with many examples of tyrosyl radicals shown to play roles in long-range electron-transfer processes,[44] most notably in photosynthesis.[45] In both docking conformations, the side chain of Y194 is close to a hydrate group of (*R*)-**5**·$H_2O$ and (*S*)-**5**·$H_2O$, suggesting that Y194 could act as a "lightning rod" for bulk solvent radicals to be funneled into the metal-binding site and directing into the cyclobutanone ring. Because the cyclobutanone hydrate moiety is already a high-energy species for reasons discussed earlier, fragmentation would be thermodynamically favorable.

**General Discussion on a Possible Mechanism for the Formation of Byproduct 6.** The exact mechanism for the formation of the cyclobutanone ring-opened byproduct **6** could not be confirmed; however, based on our model reactions, we hypothesize that the formation of **6** occurred via radiation exposure to the (±)-**5**·$H_2O$-bound AiiA complex during data collection. If AiiA alone catalyzed this ring-opening reaction, the formation of **6** would be detectable after incubations of these two molecules. We hypothesize that the formation of a radical during X-ray data collection initiated the ring-opening mechanism leading to the observed product. Additionally, Tyr194 in AiiA has been reported as a H-bond donor to stabilize the substrate's transition-state intermediate during catalysis.[16] Hence, it is reasonable to suggest that Tyr194 could participate in this reaction by stabilizing the radical involved in this mechanism, directing it selectively into the 4-membered ring system of (±)-**5**·$H_2O$. Our efforts to generate radicals using model chemical reactions in solution did not lead to the degradation of cyclobutanone (±)-**5** into the acyclic product **6**. These results suggest that the active site of AiiA may position the cyclobutanone ring of (±)-**5** in a conformation that allows only the C−C bond present between C2′and C3′ of the ring to be cleaved.

## CONCLUSIONS

We performed a detailed examination of the mechanism of AiiA-mediated hydrolysis of the homoserine lactone product-bound structures available in the PDB using our PBTSM approach to provide additional insight into the mechanism of hydrolysis of quorum-quenching lactones, augmenting our knowledge of bacterial virulence that is so critical in this era of growing antibiotic resistance. Inspired by our PBTSM analysis of the **2**-TS and **4**-TS complexes, we have designed and synthesized *N*-(2-oxocyclobutyl) decanamide (±)-**5** as a possible transition-state analogue of AiiA, which was shown to be a competitive inhibitor of dicobalt(II) AiiA with a low micromolar inhibition constant ($K_i$) of 0.007 ± 0.002 mM, suggesting that (±)-**5** captures some of the transition-state interactions stabilized by the enzyme. Soaking of the cyclobutanone substrate (±)-**5** into dicobalt(II) AiiA followed by X-ray irradiation for structural determination revealed a bound cyclobutanone ring-opened product **6** bound to dicobalt(II) AiiA (PDB 7L5F) in a novel monodentate bridge complex between the two Co(II) atoms that may represent an intermediate in the reaction. Although many methods to recreate conditions amenable to the ring-opening event were attempted, we were ultimately unsuccessful in identifying selective ring-opening conditions to produce compound **6** from cyclobutanone **5**. However, molecular docking analysis of (*R*)-**5**·$H_2O$- and (*S*)-**5**·$H_2O$-bound AiiA models suggests that Y194 may be in an optimal location to both sequester radical species from the surrounding bulk solvent and direct the radical species selectively onto the high-energy cyclobutanone moiety, whereupon fragmentation would lead to **6**. Affinity of the cyclobutanone moiety to AiiA as well as to related metallo-$\beta$-lactamases[19] suggests that this scaffold might be even more widely applicable in the development of inhibitors for diverse enzymes within this superfamily. The unexpected ring opening observed during structural characterization is intriguing in that the ring opening may have been enabled through the presence of the inhibitor in the active enzyme and may also help inform medicinal chemistry and structural efforts during the development of strained compounds. The design of cyclobutanone (±)-**5** as an intended transition-state mimetic met with success as an inhibitor of AiiA-Co but with modest potency, presumably due to the geometry of the 4-membered ring relative to the 5-membered ring of the lactone substrate, as well as its dependence on the equilibrium between the ketone and hydrate. Using the equilibrium constant for cyclobutanone as a model, which exhibits $K_{eq} = 2.18 \times 10^{-3}$ as reported by Wiberg,[46] as little as 0.2% of the inhibitor may exist in the hydrated form, suggesting that the cyclobutanone hydrate may indeed exhibit the potency expected as a transition-state mimetic. The electron-withdrawing amide substituent should increase the equilibrium somewhat relative to cyclobutanone itself, but further increasing the electrophilicity of the cyclobutanone and favoring the hydrate may be accomplished in future studies via $\alpha$-fluoro substitution, as has been demonstrated classically with trifluoromethylketone enzyme inhibitors.[47]

## ASSOCIATED CONTENT

### Supporting Information

The Supporting Information is available free of charge at https://pubs.acs.org/doi/10.1021/acsomega.0c06348.



https://doi.org/10.1021/acsomega.0c06348
ACS Omega XXXX, XXX, XXX−XXX

$^{1}$H NMR, $^{13}$C NMR, and HRMS data for cyclobutanone (±)-**5** and 4-decanamideobutanoic acid (**6**); inhibition curves of AiiA-Co by cyclobutanone (±)-**5**, crystallographic data for PDB 7L5F, plot showing lack of inhibition of AiiA-Co by acyclic amide **6**, forced degradation studies of cyclobutanone (±)-**5**, and stereoviews of PBTSM figures (PDF)

### Accession Codes

Uniprot: AiiA; Q9L8R80.
NCBI Protein: AiiA; AAY22195.
Protein Data Bank: PDB 7L5F.

## AUTHOR INFORMATION


### Corresponding Authors

**Dali Liu** − *Department of Chemistry and Biochemistry, Loyola University Chicago, Chicago, Illinois 60660, United States;* orcid.org/0000-0002-7587-703X; Email: dliu@luc.edu

**Daniel P. Becker** − *Department of Chemistry and Biochemistry, Loyola University Chicago, Chicago, Illinois 60660, United States;* orcid.org/0000-0001-9392-0460; Email: dbecke3@luc.edu

### Authors

**Cory T. Reidl** − *Department of Chemistry and Biochemistry, Loyola University Chicago, Chicago, Illinois 60660, United States*

**Romila Mascarenhas** − *Department of Chemistry and Biochemistry, Loyola University Chicago, Chicago, Illinois 60660, United States*

**Thahani S. Habeeb Mohammad** − *Department of Chemistry and Biochemistry, Loyola University Chicago, Chicago, Illinois 60660, United States*

**Marlon R. Lutz, Jr.** − *Department of Chemistry and Biochemistry, Loyola University Chicago, Chicago, Illinois 60660, United States*

**Pei W. Thomas** − *Division of Chemical Biology and Medicinal Chemistry, College of Pharmacy, The University of Texas at Austin, Austin, Texas 78712, United States*

**Walter Fast** − *Division of Chemical Biology and Medicinal Chemistry, College of Pharmacy, The University of Texas at Austin, Austin, Texas 78712, United States;* orcid.org/0000-0001-7567-2213

Complete contact information is available at: https://pubs.acs.org/10.1021/acsomega.0c06348

### Author Contributions

#C.T.R. and R.M. contributed equally to this work.


### Notes

The authors declare no competing financial interest.

## ACKNOWLEDGMENTS

This work was supported in part by the Robert A. Welch Foundation (F-1572 to WF).

## ABBREVIATIONS

AiiA, autoinducer inactivator A; PBTSM, product-based transition-state modeling

## REFERENCES


(1) World Health Organization Antibacterial agents in Clinical Development: An Analysis of the Antibacterial Clinical Development Pipeline, Including Tuberculosis. 2017, https://www.who.int/medicines/areas/rational_use/antibacterial_agents_clinical_development/en/accessed 2-22-2021.

(2) Anandan, K.; Vittal, R. R. Quorum quenching activity of AiiA lactonase KMMI17 from endophytic *Bacillus thuringiensis* KMCL07 on AHL-mediated pathogenic phenotype in *Pseudomonas aeruginosa*. *Microb. Pathog.* **2019**, *132*, 230−242.

(3) Saurav, K.; Bar-Shalom, R.; Haber, M.; Burgsdorf, I.; Steindler, L.; Oliviero, G.; Costantino, V.; Morgenstern, D. In Search of Alternative Antibiotic Drugs: Quorum-Quenching Activity in Sponges and their Bacterial Isolates. *Front. Microbiol.* **2016**, *7*, No. 416.

(4) Basavaraju, M.; Sisnity, V. S.; Palaparthy, R.; Addanki, P. K. Quorum quenching: Signal jamming in dental plaque biofilms. *J. Dent. Sci.* **2016**, *11*, 349−352.

(5) Chu, Y.; Nega, M.; Wölfle, M.; Plener, L.; Grond, S.; Jung, K.; Götz, F. A New Class of Quorum Quenching Molecules from *Staphylococcus* Species Affects Communication and Growth of Gram-Negative Bacteria. *PLoS Pathog.* **2013**, *9*, No. e1003654.

(6) Guendouze, A.; Plener, L.; Bzdrenga, J.; Jacquet, P.; Rémy, B.; Elias, M.; Lavigne, J.; Daudé, D.; Chabrière, E. Effect of Quorum Quenching Lactonase in Clinical Isolates of *Pseudomonas aeruginosa* and Comparison with Quorum Sensing Inhibitors. *Front. Microb.* **2017**, *8*, No. 227.

(7) Fetzner, S. Quorum quenching enzymes. *J, Biotechnol.* **2015**, *201*, 2−14.

(8) Dong, Y.; Xu, J.; Li, X.; Zhang, L. AiiA, an enzyme that inactivates the acylhomoserine lactone quorum-sensing signal and attenuates the virulence of *Erwinia carotovora*. *Proc. Natl. Acad. Sci. U.S.A.* **2000**, *97*, 3526−3531.

(9) Wang, W. Z.; Morohoshi, T.; Someya, N.; Ikeda, T. AidC, a novel *N*-acylhomoserine lactonase from the potato root-associated cytophaga-flavobacteria-bacteroides (CFB) group bacterium *Chryseobacterium sp.* strain StRB126. *Appl. Environ. Microbiol.* **2012**, *78*, 7985−7992.

(10) Mascarenhas, R.; Thomas, P. W.; Wu, C.; Nocek, B. P.; Hoang, Q. Q.; Liu, D.; Fast, W. Structural and Biochemical Characterization of AidC, a Quorum-Quenching Lactonase with Atypical Selectivity. *Biochemistry* **2015**, *54*, 4342−4353.

(11) Liu, D.; Lepore, B. W.; Petsko, G. A.; Thomas, P. W.; Stone, E. M.; Fast, W.; Ringe, D. Three-dimensional structure of the quorum-quenching *N*-acyl homoserine lactone hydrolase from *Bacillus thuringiensis*. *Proc. Natl. Acad. Sci. U.S.A.* **2005**, *102*, 11882−11887.

(12) Liao, R.; Yu, J.; Himo, F. Reaction Mechanism of the Dinuclear Zinc Enzyme *N*-Acyl-L-homoserine Lactone Hydrolase: A Quantum Chemical Study. *Inorg. Chem.* **2009**, *48*, 1442−1448.

(13) Ben-David, M.; Wieczorek, G.; Elias, M.; Silman, I.; Sussman, J. L.; Tawfik, D. S. Catalytic Metal Ion Rearrangements Underline Promiscuity and Evolvability of a Metalloenzyme. *J. Mol. Biol.* **2013**, *425*, 1028−1038.

(14) Dong, Y.; Zhang, L. Quorum sensing and quorum-quenching enzymes. *J. Microbiol.* **2005**, *43*, 101−109.

(15) Liao, R.; Yu, J.; Himo, F. Reaction Mechanism of the Dinuclear Zinc Enzyme *N*-Acyl-L-homoserine Lactone Hydrolase: A Quantum Chemical Study. *Inorg. Chem.* **2009**, *48*, 1442−1448.

(16) Momb, J.; Wang, C.; Liu, D.; Thomas, P. W.; Petsko, G. A.; Guo, H.; Ringe, D.; Fast, W. Mechanism of the Quorum-Quenching Lactonase (AiiA) from *Bacillus thuringiensis*. 2. Substrate Modeling and Active Site Mutations. *Biochemistry* **2008**, *47*, 7715−7725.

(17) Liu, D.; Momb, J.; Thomas, P. W.; Moulin, A.; Petsko, G. A.; Fast, W.; Ringe, D. Mechanism of the quorum-quenching lactonase (AiiA) from *Bacillus thuringiensis*. 1. Product-bound structures. *Biochemistry* **2008**, *47*, 7706−7714.

(18) Liu, C. F.; Liu, D.; Momb, J.; Thomas, P. W.; Lajoie, A.; Petsko, G. A.; Fast, W.; Ringe, D. A Phenylalanine Clamp Controls Substrate Specificity in the Quorum-Quenching Metallo-γ-lactonase from *Bacillus thuringiensis*. *Biochemistry* **2013**, *52*, 1603−1610.

(19) Johnson, J. W.; Gretes, M.; Goodfellow, V. J.; Marrone, L.; Heynen, M. L.; Strynadka, N. C. J.; Dmitrienko, G. I. Cyclobutanone analogues of β-lactams revisited: Insights into conformational



https://doi.org/10.1021/acsomega.0c06348
ACS Omega XXXX, XXX, XXX−XXX

requirements for inhibition of serine- and metallo-β-lactamases. *J. Am. Chem. Soc.* **2010**, *132*, 2558−2560.
(20) Abboud, M. I.; Kosmopoulou, M.; Krismanich, A.; Johnson, J. W.; Hinchliffe, P.; Brem, J.; Claridge, T. D.; Spencer, J.; Schofield, C.; Dmitrienko, G. I. Cyclobutanone Mimics of Intermediates in Metallo-β-Lactamase Catalysis. *Chem. - Eur. J.* **2017**, *24*, 5734−5737.
(21) Filippova, E. V.; Weston, L. A.; Kuhn, M. L.; Geissler, B.; Gehring, A. M.; Armoush, N.; Adkins, C. T.; Minasov, G.; Dubrovska, I.; Shuvalova, L.; Winsor, J. R.; Lavis, L. D.; Satchell, K. J. F.; Becker, D. P.; Anderson, W. F.; Johnson, R. J. Large Scale Structural Rearrangement of a Serine Hydrolase from *Francisella tularensis* Facilitates Catalysis. *J. Biol. Chem.* **2013**, *288*, 10522−10535.
(22) Mohammad, T. S. H.; Reidl, C. T.; Zeller, M.; Becker, D. P. Synthesis of a protected 2-aminocyclobutanone as a modular transition state synthon for medicinal chemistry. *Tetrahedron Lett.* **2020**, *61*, No. 151632.
(23) Momb, J.; Thomas, P. W.; Breece, R. M.; Tierney, D. L.; Fast, W. The quorum-quenching metallo-γ-lactonase from *Bacillus thuringiensis* exhibits a leaving group thio effect. *Biochemistry* **2006**, *45*, 13385−13393.
(24) Armoush, N.; Syal, P.; Becker, D. P. Synthesis of substituted 2-aminocyclobutanones. *Synth. Commun.* **2008**, *38*, 1679−1687.
(25) Riva, E.; Wilkening, I.; Gazzola, S.; Li, W. M. A.; Smith, L.; Leadlay, P. F.; Tosin, M. Chemical Probes for the Functionalization of Polyketide Intermediates. *Angew. Chem., Int. Ed.* **2014**, *53*, 11944−11949.
(26) Elioff, M. S.; Hoy, J.; Bumpus, J. A. Calculating heat of formation values of energetic compounds: A comparative study. *Adv. Phys. Chem.* **2016**, *2016*, 1−11.
(27) Thomas, P. W.; Fast, W. Heterologous Overexpression, Purification, and In Vitro Characterization of AHL Lactonases. In *Quorum Sensing: Methods in Molecular Biology (Methods and Protocols)*; Rumbaugh, K., Ed.; Humana Press, 2011; Vol. *692*.
(28) Rutherford, S. T.; Bassler, B. L. Bacterial quorum sensing: its role in virulence and possibilities for its control. *Cold Spring Harbor Perspect. Med.* **2012**, *2*, No. a012427.
(29) Minor, W.; Cymborowski, M.; Otwinowski, Z.; Chruszcz, M. HKL-3000: the integration of data reduction and structure solution−from diffraction images to an initial model in minutes. *Acta Crystallogr., Sect. D: Biol. Crystallogr.* **2006**, *62*, 859−866.
(30) Adams, P. D.; Afonine, P. V.; Bunkóczi, G.; Chen, V. B.; Davis, I. W.; Echols, N.; Headd, J. J.; Hung, L.; Kapral, G. J.; Grosse-Kunstleve, R.; McCoy, A. J.; Moriarty, N. W.; Oeffner, R.; Read, R. J.; Richardson, D. C.; Richardson, J. S.; Terwilliger, T. C.; Zwart, P. H. PHENIX: a comprehensive Python-based system for macromolecular structure solution. *Acta Crystallogr., Sect. D: Biol. Crystallogr.* **2009**, *66*, 213−221.
(31) Emsley, P.; Lohkamp, B.; Scott, W. G.; Cowtan, K. Features and development of Coot. *Acta Crystallogr., Sect. D: Biol. Crystallogr.* **2010**, *66*, 486−501.
(32) Pettersen, E. F.; Goddard, T. D.; Huang, C. C.; Couch, G. S.; Greenblatt, D. M.; Meng, E. C.; Ferrin, T. E. UCSF Chimera-A visualization system for exploratory research and analysis. *J. Comput. Chem.* **2004**, *25*, 1605−1612.
(33) Lebedev, A. A.; Young, P.; Isupov, M. N.; Moroz, O. V.; Vagin, A. A.; Murshudov, G. N. JLigand: a graphical tool for the CCP4 template-restraint library. *Acta Crystallogr., Sect. D: Biol. Crystallogr.* **2012**, *68*, 431−440.
(34) CCGI M. *Molecular Operating Environment (MOE)*, 2013.08; Chemical Computing Group Inc.: 1010 Sherbooke St. West, Suite #910: Montreal, QC, Canada, H3A 2R7, 2018.
(35) Reidl, C.; Majorek, K. A.; Dang, J.; Tran, D.; Jew, K.; Law, M.; Payne, Y.; Minor, W.; Becker, D. P.; Kuhn, M. L. Generating enzyme and radical-mediated bisubstrates as tools for investigating Gcn5-related *N*-acetyltransferases. *FEBS Lett.* **2017**, *591*, 2348−2361.
(36) Nocek, B.; Reidl, C.; Starus, A.; Heath, T.; Bienvenue, D.; Osipiuk, J.; Jedrzejczak, R. P.; Joachimiak, A.; Becker, D. P.; Holz, R. C. Structural Evidence for a Major Conformational Change Triggered by Substrate Binding in DapE Enzymes: Impact on the Catalytic Mechanism. *Biochemistry* **2018**, *57*, 574−584.
(37) Labute, P. The generalized Born/volume integral implicit solvent model: Estimation of the free energy of hydration using London dispersion instead of atomic surface area. *J. Comput. Chem.* **2008**, *29*, 1693−1698.
(38) Burmeister, W. P. Structural changes in a cryo-cooled protein crystal owing to radiation damage. *Acta Crystallogr., Sect. D: Biol. Crystallogr.* **2000**, *56*, 328−341.
(39) Wood, G. P.; Moran, D.; Jacob, R.; Radom, L. Bond dissociation energies and radical stabilization energies associated with model peptide-backbone radicals. *J. Phys. Chem. A* **2005**, *109*, 6318−6325.
(40) Namyslo, J. C.; Kaufmann, D. E. The Application of Cyclobutane Derivatives in Organic Synthesis. *Chem. Rev.* **2003**, *103*, 1485−1537.
(41) Chaumeil, H.; Le Drian, C. Preparation of α,α-Dibromocyclobutanones from Olefins: A simple procedure for the regioselective functionalization of olefins. *Helv. Chim. Acta* **1996**, *79*, 1075−1084.
(42) Jaffer, M.; Ebead, A.; Lee-Ruff, E. Photochemical synthesis of nucleoside analogues from cyclobutanones: bicyclic and isonucleosides. *Molecules* **2010**, *15*, 3816−3828.
(43) Walling, C. Fenton's reagent revisited. *Acc. Chem. Res.* **1975**, *8*, 125−131.
(44) Range, K.; Ayala, I.; York, D.; Barry, B. A. Normal Modes of Redox-Active Tyrosine: Conformation Dependence and Comparison to Experiment. *J. Phys. Chem. B* **2006**, *110*, 10970−10981.
(45) Nakamura, S.; Capone, M.; Narzi, D.; Guidoni, L. Pivotal role of the redox-active tyrosine in driving the water splitting catalyzed by photosystem II. *Phys. Chem. Chem. Phys.* **2020**, *22*, 273−285.
(46) Wiberg, K. B.; Morgan, K. M.; Maltz, H. Thermochemistry of carbonyl reactions. 6. A study of hydration equilibria. *J. Am. Chem. Soc.* **1994**, *116*, 11067−11077.
(47) Gelb, M. H.; Svaren, J. P.; Abeles, R. H. Fluoro ketone inhibitors of hydrolytic enzymes. *Biochemistry* **1985**, *24*, 1813−1817.


https://doi.org/10.1021/acsomega.0c06348
*ACS Omega* XXXX, XXX, XXX−XXX